***Proceedings of the IASS 2024 Symposium***
*Redefining the Art of Structural Design*
August 26-30, 2024, Zurich Switzerland
Philippe Block, Giulia Boller, Catherine DeWolf,
Jacqueline Pauli, Walter Kaufmann (eds.)

# Discrete thickness optimization for free-form shell structures based on multi-material topology optimization

Yu LI[a], Xinjie ZHOU[a], Philip F. YUAN[a,*]

[a,*] College of Architecture and Urban Planning, Tongji University, Shanghai, 200092, China

[*] philipyuan007@tongji.edu.cn

## Abstract

In the field of lightweight free-form shell design, the optimization of thickness plays an important role in ensuring both light weight and adequate stiffness. For traditional construction methods, designing variable discrete shell thicknesses is a practical approach for successful implementation. To achieve this goal, a novel thickness optimization method for shells based on the multi-material bi-directional evolutionary structural optimization (BESO) method is proposed in this study. As a proof of concept, a shell pavilion prototype measuring approximately 12 m × 8 m × 5 m is designed. By comparing various free-form shell designs with different thickness distributions and considering factors such as the Young's modulus and the number of materials, this study demonstrates the effectiveness of the proposed method in achieving lightweight design with adequate structural efficiency. The discrete thickness optimization for the shell case in this paper confirms the potential application of multi-material topology optimization methods in the lightweight design of shell structures.

**Keywords**: Multi-material topology optimization, shell design, thickness optimization, lightweight design.

## 1. Introduction

Shell structure is an important form in in architectural design, offering the potential for expansive interior spaces, heightened clear heights, and reduced weight through thoughtful engineering[1–3]. The optimization of free-form shell structures is essential for enhancing structural efficiency, particularly through lightweight design, which minimizes the structure's self-weight without compromising its efficiency [4,5]. Optimization strategies typically center around geometry [6–9], topology [10–13], thickness [14,15], or integrated optimization [16–18]. While past research has predominantly emphasized continuous thickness optimization, such approaches have posed challenges in terms of constructability.

This paper introduces a novel approach to optimize the thickness of free-form shell structures using multi-material topology optimization techniques. Building upon the bi-directional evolutionary structural optimization (BESO) method [19], our technique incorporates gradient distribution strategies for different materials, allowing for the distribution of high and low-performance materials gradients. Our preliminary research demonstrates the potential of the multi-material BESO method in designing high-performance building structures [20–22]. It effectively optimizes topology for multiple linear and nonlinear materials and has shown promising results in practical engineering structural design applications [23–25]. Leveraging multi-material BESO method, the paper focuses on optimizing the thickness of free-form shell structures. The topologically optimized shell structure features a limited

number of thickness variations, streamlining subsequent construction design and implementation processes.

## 2. Multi-material topology optimization

### 2.1 Problem statement

The multi-material BESO method utilized in this study [26] is an extension algorithm based on the single-material BESO method. The various materials investigated in this study are all linear and isotropic, denoted as $M_1$, $M_2$, …, $M_n$, assuming these materials have the following Young's moduli: $E_1$, $E_2$, ..., $E_n$ (where $E_1 > E_2 \cdots > E_n$). The topology optimization problem for structures composed of these multiple materials can be stated as:

$$\text{minimize: } C = \frac{1}{2}\mathrm{u}^{\boldsymbol{T}}\mathrm{Ku} \tag{1a}$$

$$\text{subject to: } V_j^* - \sum_{i=1}^{N} V_i\, x_{ij} - \sum_{i=1}^{j-1} V_i^* = 0 \tag{1b}$$

$$x_{ij} = x_{\min} \text{ or } 1 \ (j = 1, 2, \ldots, n\text{-}1) \tag{1c}$$

where the optimization objective is to minimize the compliance $C$, and $\mathbf{K}$ and $\mathbf{u}$ represent the global stiffness matrix of the structure and displacement vectors respectively. $V_i$ is the volume of an individual element, and $V_j^*$ is the prescribed total structural volume. The binary design variable $x_{ij}$ denotes the density of the $i$-th element, taking values of either $x_{\min}$ or 1. Here, $x_{\min}$ represents a small value ($10^{-6}$ is set in this study) used to avoid singularity in the stiffness matrix.

For the $j$-th material among the n materials, design variables $x_{ij}$ are introduced to denote the density of the $i$-th element for the $j$-th material, satisfying:

$$x_{ij} = \begin{cases} 1 & \text{for } E \geq E_j \\ x_{\min} & \text{for } E < E_j \end{cases} \tag{2}$$

Following previous research [26], sensitivity analysis is computed as follows:

$$\alpha_{ij} = \begin{cases} \frac{1}{2}\left[1 - \frac{E_{j+1}}{E_j}\right] \mathrm{u_i}^{\mathrm{T}}\mathrm{Ku_i} & \text{for material } 1, \ldots, j \\ 0 & \text{for material } j+1, \ldots, n \end{cases} \tag{3}$$

It is observed that there are $n - 1$ groups of sensitivity numbers in the system to adjust neighboring materials.

### 2.2 Process of the multi-material BESO method

Similar to the single-material "solid-void" BESO method [27,28], the process of multi-material topology optimization in this study is outlined as follows:

**Step 1**: Discretize the design domain into finite element analysis (FEA) mesh.

**Step 2**: Set the topology optimization parameters for the BESO method, including the target volume fraction $V^*$, evolution rate $ER$, filtering radius $R_{\min}$, convergence control parameter $\tau$, etc.

**Step 3**: Perform FEA to compute sensitivity number for each element.

**Step 4**: Construct exponential functions to calculate the next step's target volume until the volume reaches to the target volume fraction $V^*$ and remains unchanged.

**Step 5**: Compute the threshold sensitivity numbers for each material; assign $x$ values of 1 to elements with sensitivity numbers greater than the threshold; otherwise, assign $x$ values of $x_{\min}$.

**Step 6**: Repeat steps 3-5 until the structure reaches the target volume fraction and converges.

## 3 Multi-material topology optimization for 2D cantilevers

### 3.1 Cantilever with two non-zero materials

Firstly, verification is conducted using a 2D short cantilever, as illustrated in Figure 1. The dimensions of the short cantilever beam are 100 mm × 60 mm, with a finite element mesh of 200 × 120. The left side of the cantilever beam is fully fixed, while a concentrated force $F$ = 100 N is applied on the right side. Two non-zero materials are employed in the topology optimization process: material $M_1$ with a Young's modulus $E_1$ = 200 GPa and material $M_2$ with $E_2$ = 20 GPa, both having a Poisson's ratio of $v$ = 0.3. The evolution rate is set to $ER$ = 0.01, with target volume fractions of $v_{f1}$ = 0.5 and vf2 = 0.5, indicating an equal proportion of the two materials in the final structure. The filter radius is set to r = 2 mm.

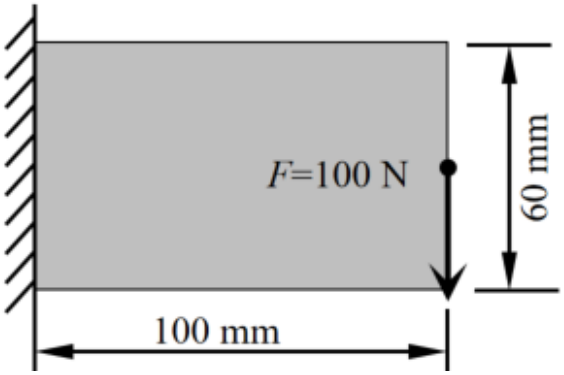


Figure 1: Design domain, support and load configurations for the 2D short cantilever.

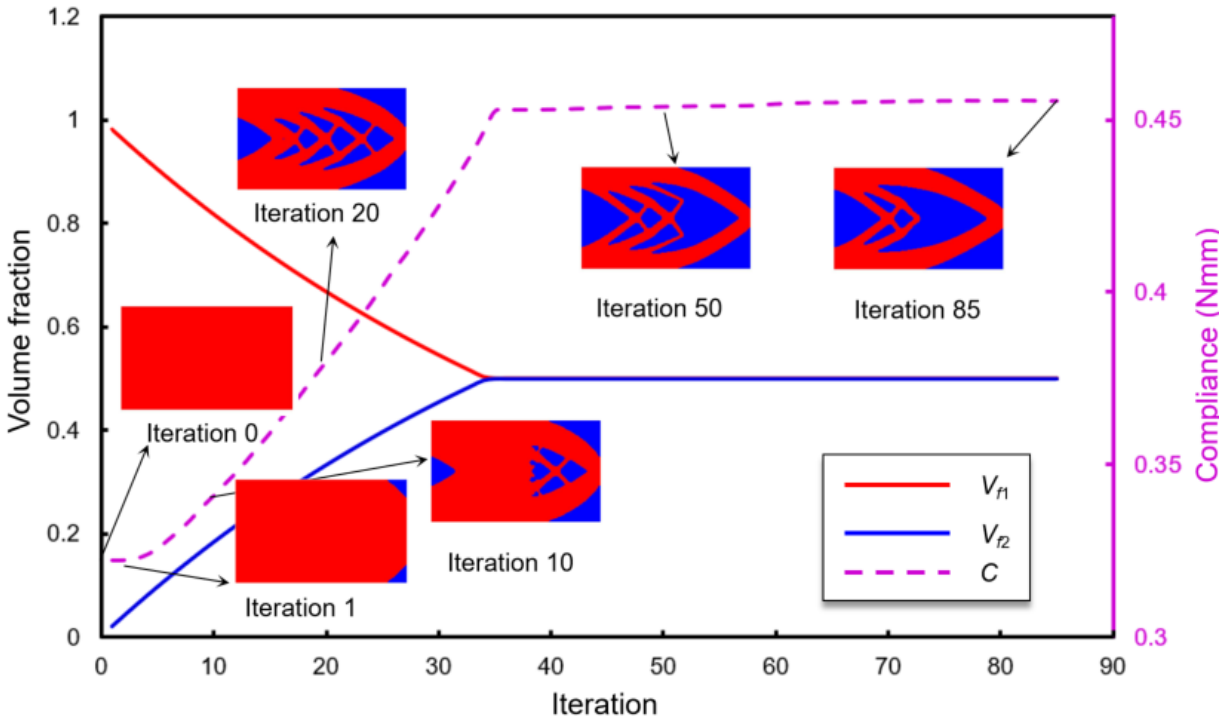


Figure 2: Evolutionary histories of compliance, volume fractions, and topology of the cantilever.

The entire evolutionary process of the topology optimization is illustrated in Figure 2. Initially (Iteration 0), as shown, the entire design domain is composed of material $M_1$ (red). As the topology optimization progresses, the proportion of the weaker material $M_2$ (blue) begins to increase. After 35 iterations, the volume fractions of the two materials become equal, each accounting for 50%. Following this, the volume fractions remain constant, and the structure gradually converges.

### 3.2 Effect of relative ratio of Young's modulus of two non-zero materials on the results of topology optimization

To explore the influence of the relative ratio of Young's modulus between the two non-zero materials on the results of topology optimization, a series of variations in Young's modulus ratio are set. $E_1$ is kept constant at 200 GPa, while $E_2$ is respectively set to $2 \times 10^{-4}$ GPa, 20 GPa, and 100 GPa. All other parameters remain consistent with the settings in the case depicted in Figure 2. The topology optimization results obtained based on these settings are illustrated in Figure 3.

It can be observed that when there is a significant difference in Young's modulus between the two materials (say $E_1$: $E_2 = 1{:}10^{-6}$), the optimal topology of this dual-material cantilever is very similar to the result of a single-material short cantilever. In fact, when using the "soft-kill" BESO method [19] for "solid-void" topology optimization, setting void elements to have a material with $E = E_{\min}$ can be considered equivalent to the scenario presented here in Figure 3(a). Thus, "solid-void" single-material topology optimization can be regarded as a special case of non-zero two-phase material topology optimization.

Furthermore, as the Young's modulus of material $M_2$ increases, the optimal topology of the structure changes. When $E_1$: $E_2 = 1{:}10^{-6}$, the topology of material $M_1$ is very simple, with only major components composed of $M_1$, unlike the topology with $E_1$: $E_2 = 1{:}10^{-6}$, where the structure exhibits many branches. Additionally, as the Young's modulus of $M_2$ increases, the total compliance of the structure gradually decreases. Therefore, it can be seen that the difference in Young's modulus between the two materials has a significant impact on the optimal topology of the structure.

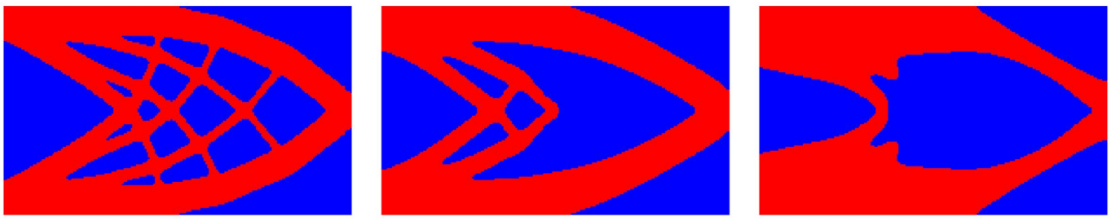

(a) $E_1 : E_2 = 1{:}10^{-6}$, $E_1 = 200$ GPa, $E_2 = 200$ MPa, $C = 1.01$ Nmm

(b) $E_1 : E_2 = 1{:}0.1$, $E_1 = 200$ GPa, $E_2 = 20$ GPa, $C = 0.93$ Nmm

(c) $E_1 : E_2 = 1{:}0.5$, $E_1 = 200$ GPa, $E_2 = 100$ GPa, $C = 0.73$ Nmm

Figure 3: Two-material 2D cantilevers with varying relative ratios of Young's modulus optimized using multi-material BESO.

### 3.3 Effect of material quantity variation on multi-material topology optimization.

When the method is extended to incorporate more materials, it yields a wider range of results. As depicted in Figure 4, topology optimizations are conducted for the same cantilever with 2, 3, and 4 materials, respectively. The Young's modulus of materials in these cases is set as follows: (a) $E_1$: $E_2$ = 10:1; (b) $E_1$: $E_2$: $E_3$ = 1:0.1:0.01; (c) $E_1$: $E_2$: $E_3$: $E_4$ = 1:0.1:0.01:0.001. In each case, the target volume fractions for all sub-materials are equal. Other parameters remain consistent with those in Figure 2.

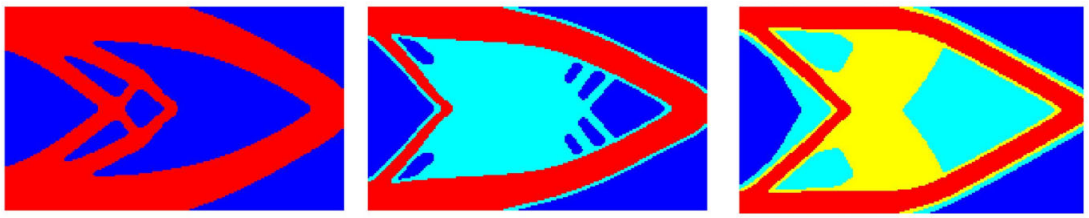

(b) $E_1 : E_2 = 1{:}0.1$, $E_1 = 200$ GPa, $E_2 = 20$ GPa, $C = 0.93$ Nmm

(b) $E_1 : E_2 : E_3 = 1{:}0.1{:}0.01$ $E_1 = 200$ GPa, $E_2 = 20$ GPa, $E_3 = 2$ GPa, $C = 1.14$ Nmm

(c) $E_1 : E_2 : E_3 : E_4 = 1{:}0.1{:}0.01{:}0.001$ $E_1 = 200$ GPa, $E_2 = 20$ GPa, $E_3 = 2$ GPa, $E_4 = 0.2$ GPa, $C = 1.41$ Nmm

Figure 4: 2D cantilevers optimized using multi-material BESO with 2, 3, and 4 materials.

It can be observed that the results of topology optimization in Figure 4 indicate that the number of materials significantly influences the optimal topology of the structure. Additionally, as the number of materials with lower Young's modulus increases, the compliance of the structure gradually rises. This structural weakening is mainly caused by the reduction in the usage of high-performance materials, thus reducing structural costs. This advantage holds significant implications for cost control in practical engineering structures.

## 4. Thickness optimization for free-form shells

### 4.1 Thickness optimization of free-form shells with two different thicknesses

The algorithm mentioned above, when applied to 3D shell structures, yields lightweight and efficient shell forms. The free-form shell to be optimized is depicted in Figure 5, with geometric dimensions of 12 m × 8 m × 5 m. The shell is discretized into 8960 quadrilateral elements for FEA. The thickness of the shell is set as $t$ = 50 mm. PLA material is planned for 3D printing construction of the free-form shell. The material properties are set as follows: modulus $E$ = 4 GPa, density $\rho$ = 1.43 g/cm$^3$, and Poisson's ratio $v$ = 0.3.

In this topology optimization example, only the self-gravity acting on the shell is considered. All positions where the shell contacts the ground are set to be fully fixed. The evolution ratio for topology optimization is set to $ER$ = 0.01, and the filter radius is set to $r_{\min}$ = 600 mm. The target volume fractions for both materials are set to $v_{f1}$ = 0.5 and $v_{f2}$ = 0.5.

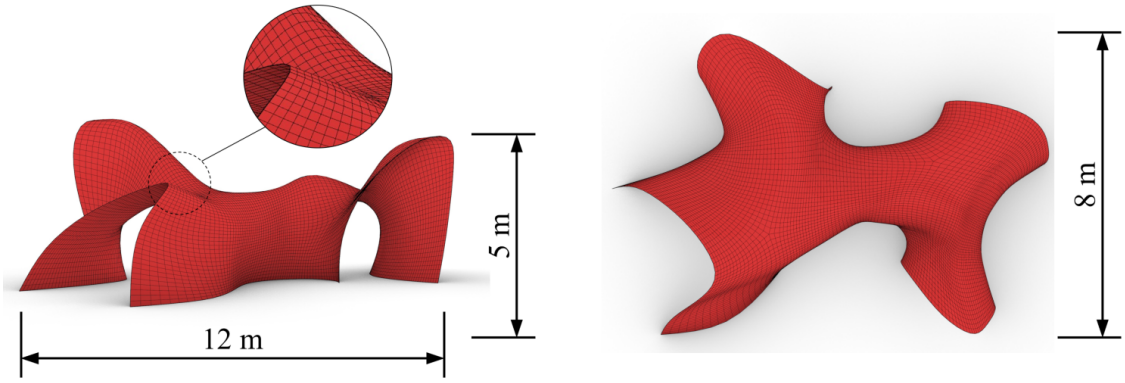


Figure 5: Front and top views of the free-form shell to be optimized.

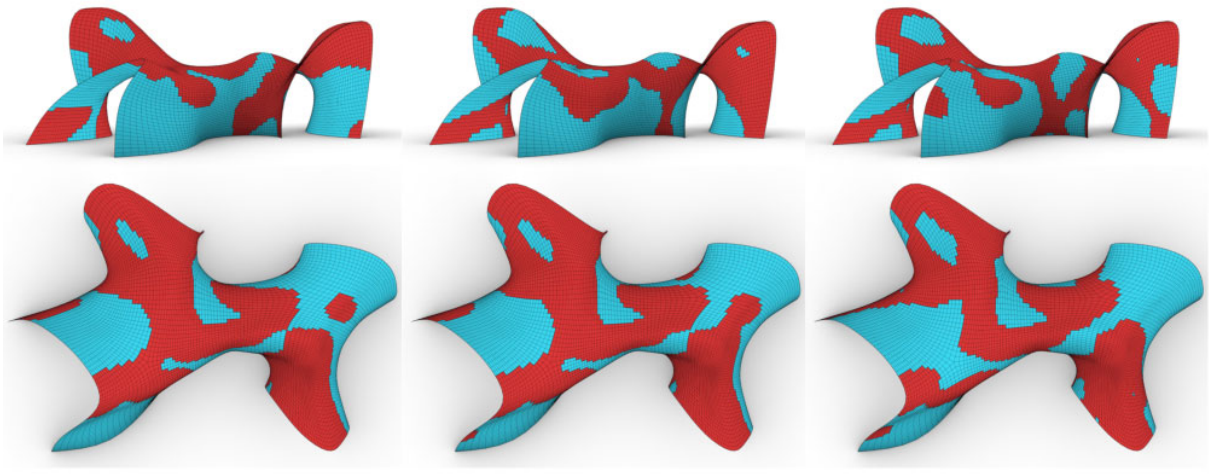


Figure 6: Free-form shells with two different thicknesses optimized using multi-material BESO.

The shell's topology optimization is firstly conducted by using two materials. Two materials with varying Young's moduli donate shell components with different thicknesses. For instance, $E_2$ = 2 GPa represents a thickness of $t$ = 25 mm. This proportional substitution is a simplification; strictly speaking, it requires rigorous finite element analysis or loading tests to determine the actual ratio of Young's moduli. In this paper, only a simplified linear relationship is utilized to demonstrate the feasibility of using a multi-material topology optimization method for discretized thickness optimization of shells.

The results of the topology optimization using two materials are depicted in Figure 6. Material M2, donating the thinner thickness material, is utilized in these cases, with Young's moduli of $E_2$ = 2 GPa, 0.4 GPa, and 0.04 GPa for thicknesses of 25 mm, 5 mm, and 0.5 mm, respectively. It is noticeable that the distribution of materials exhibits some variation due to the differing ratios of Young's moduli between the two materials. Additionally, as the Young's modulus of material M2 decreases, the overall compliance of the structure gradually increases.

### 4.2 Thickness optimization of free-form shells with multiple different thicknesses.

Furthermore, this paper conducts additional topology optimization for the free-form shell using a different number of materials, as illustrated in Figure 7. Specifically, topology optimization is performed using 2, 3, and 4 different materials, with Young's moduli $E_1$ = 4 GPa, $E_2$ = 2 GPa, $E_3$ = 1 GPa, and $E_4$ = 0.5 GPa, representing thicknesses of 50 mm, 25 mm, 12.5 mm, and 6.25 mm, respectively.

The topology optimization settings remain consistent with those of the case in Figure 6. In each case, the target volume fraction for each material is set to be equal. That is, in the bi-material structure, the target volume fraction for each material is 0.5; in the tri-material structure, it is 0.33 for each material; and in the quad-material structure, it is 0.25 for each material. After employing the multi-material BESO method, the optimal topologies shown in Figure 7 are obtained.

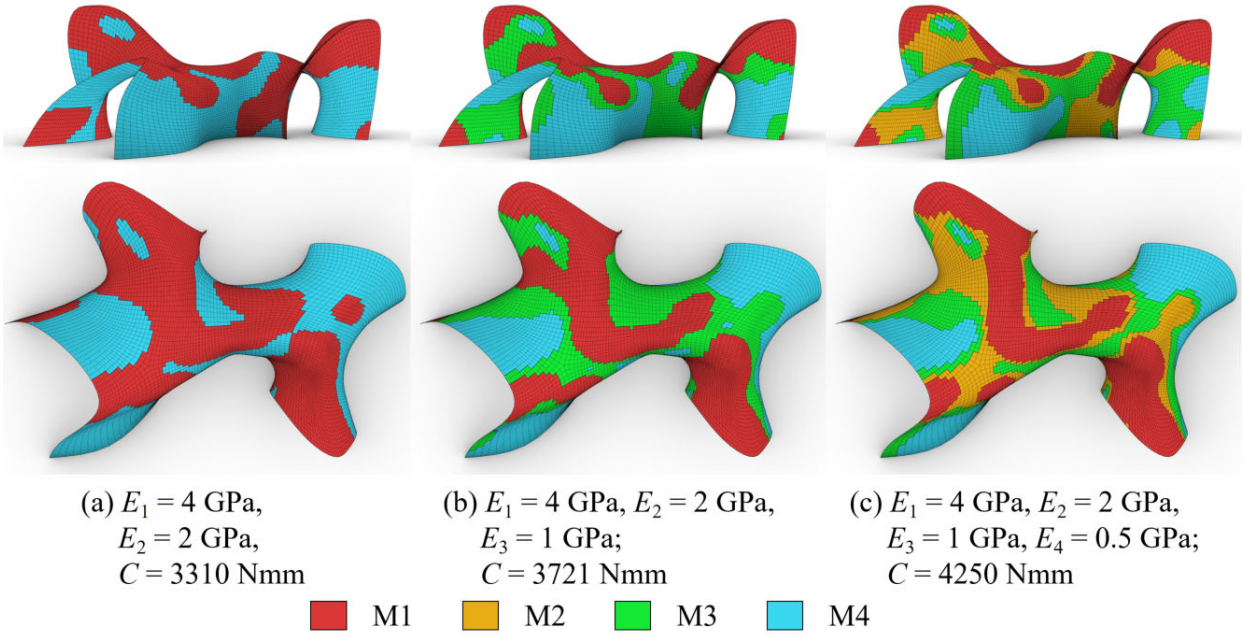


Figure 7: Free-form shells with various thicknesses optimized using multi-material BESO.

It can be observed that these structures exhibit significant differences, with richer details emerging as the number of materials increases. Comparing the compliance of these structures reveals that, with an increase in the number of materials, the volume fraction of high-performance sub-materials within the structure gradually decreases, leading to a gradual increase in the compliance of the shell structure. Similar to the 2D cantilever example, although the overall stiffness of the structure decreases, there is a potential for overall cost reduction, warranting further investigation.

## 5. Conclusion

The multi-material topology optimization algorithm proves to be capable of achieving optimal designs for multiphase material structures under given material volume constraints, demonstrating tremendous potential in the lightweight design of shell structures. This study, focusing on 2D short cantilevers firstly, investigated the influence of sub-material Young's modulus variations on the optimal topology and structural performance within the framework of the multi-material bi-directional evolutionary structural optimization (BESO) method. Furthermore, the research delved into the variations in optimal topology and structural performance of multi-material short 2D cantilevers with different numbers of sub-materials, providing insights into the relationship between these variables. Moreover, based on the insights gained from the 2D short cantilever study, this multi-material BESO approach is applied to optimize a free-form shell measuring 12 m × 8 m × 5 m, achieving discrete thickness optimization of the shell under various material property settings and thickness quantities. These preliminary studies provide a basis for further refinement in shell design, offering a novel approach to lightweight design in shell structures.

## Acknowledgements

This study was funded by the National Key Research and Development Program of China (2023YFC3806900), Ministry of Housing and Urban-Rural Development (2021-R-085), and the Science and Technology Commission of Shanghai Municipality 2021 “Science and Technology Innovation Action Plan Social Development Technological Tackling Project” (21DZ1204500).

## References

[1] M. Farshad, *Design and Analysis of Shell Structures*, Springer, 1992.

[2] M. Gohnert, *Shell Structures: Theory and Application*. Springer, 2022.

[3] Y. Li and L. Yang, “Research and application of a new super-long span roof based on cable structure,” *Structural Design of Tall and Special Buildings*, vol. 28, no. 10, pp. 1616, 2019.

[4] E. Ramm, K. U. Bletzinger, and R. Reitinger, “Shape optimization of shell structures,” *Revue Européenne des Éléments Finis*, vol. 2, no. 3, pp. 377–398, 1993.

[5] S. Adriaenssens, P. Block, D. Veenendaal, and C. Williams (eds.), *Shell structures for architecture: Form finding and optimization*, Routledge, 2014.

[6] C. Kupwiwat, K. Hayashi, and M. Ohsaki, “Deep deterministic policy gradient and graph attention network for geometry optimization of latticed shells,” *Applied Intelligence*, vol. 53, no. 17, pp. 19809–19826, 2023.

[7] P. Block, T. Van Mele, and M. Rippmann, “Structural stone surfaces: New compression shells inspired by the past,” *Architectural Design*, vol. 85, no. 5, pp. 74–79, 2015.

[8] D. Veenendaal and P. Block, “An overview and comparison of structural form finding methods for general networks,” *International Journal of Solids and Structures*, vol. 49, no. 26, pp. 3741-3753, 2012.

[9] P. F. Yuan et al., “Robotic 3D printed lunar bionic architecture based on lunar regolith selective laser sintering technology,” *Architectural Intelligence*, vol. 1, no. 1, pp. 1–17, 2022.

[10] J. Ma, H. Lu, T.-U. Lee, Y. Liu, D. W. Bao, and Y. M. Xie, “Topology optimization of shell structures in architectural design,” *Architectural Intelligence*, vol. 2, no. 1, pp. 1–12, 2023.

[11] T. Ho-Nguyen-Tan and H. G. Kim, “An efficient method for shape and topology optimization of shell structures,” *Structural and Multidisciplinary Optimization*, vol. 65, no. 4, pp. 119, 2022.

[12] S. Xu, J. Liu, J. Huang, B. Zou, and Y. Ma, "Multi-scale topology optimization with shell and interface layers for additive manufacturing," *Additive Manufacturing*, vol. 37, pp. 101698, 2021.

[13] X. Wang et al., "3D-printed bending-active formwork for shell structures," *Architectural Intelligence*, pp. 295–314, 2020.

[14] X. Wang, C. Zhang, T. Liu, W. Liao, and C. Wang, "Variable-thickness optimization method for shell structures based on a regional evolutionary control strategy," *Thin-Walled Structures*, vol. 172, pp. 108848, 2022.

[15] G. Weldeyesus and M. Stolpe, "Free material optimization for laminated plates and shells," *Structural and Multidisciplinary Optimization*, vol. 53, no. 6, pp. 1335–1347, 2016.

[16] X. Meng, Y. Xiong, Y. M. Xie, Y. Sun, and Z. Zhao, "Shape–thickness–topology coupled optimization of free-form shells," *Automation in Construction*, vol. 142, pp. 104476, 2022.

[17] Y. Xia, Y. Wu, and M. A. N. Hendriks, "Simultaneous optimization of shape and topology of free-form shells based on uniform parameterization model," *Automation in Construction*, vol. 102, pp. 148-159, 2019.

[18] B. Hassani, S. M. Tavakkoli, and H. Ghasemnejad, "Simultaneous shape and topology optimization of shell structures," *Structural and Multidisciplinary Optimization*, vol. 48, no. 1, pp. 221–233, 2013.

[19] X. Huang and Y. M. Xie, *Evolutionary topology optimization of continuum structures: methods and applications*. Wiley, 2010.

[20] Y. Li and Y. M. Xie, "Evolutionary topology optimization for structures made of multiple materials with different properties in tension and compression," *Composite Structures*, vol. 259, pp. 113497, 2021.

[21] Y. Li, P. F. Yuan, and Y. M. Xie, "Topology optimization of structures composed of more than two materials with different tensile and compressive properties," *Composite Structures*, vol. 306, pp. 116609, 2023.

[22] Y. Li, P. F. Yuan, and Y. M. Xie, "A strategy for improving the safety and strength of topologically optimized multi-material structures," *Acta Mechanica Sinica*, vol. 39, no. 8, pp. 422134, 2023.

[23] Y. Li et al., "Practical application of multi-material topology optimization to performance-based architectural design of an iconic building," *Composite Structures*, 2023.

[24] Y. Li, Y. Lai, G. Lu, F. Yan, P. Wei, and Y. M. Xie, "Innovative design of long-span steel–concrete composite bridge using multi-material topology optimization," *Engineering Structures*, vol. 269, pp. 114838, 2022.

[25] Y. Li, H. Wu, X. Xie, L. Zhang, P. F. Yuan, and Y. M. Xie, "FloatArch: A cable-supported, unreinforced, and re-assemblable 3D-printed concrete structure designed using multi-material topology optimization," *Additive Manufacturing*, vol. 81, pp. 104012, 2024.

[26] X. Huang and Y. M. Xie, "Bi-directional evolutionary topology optimization of continuum structures with one or multiple materials," *Computational Mechanics*, vol. 43, no. 3, pp. 393–401, 2009.

[27] M. Querin, V. Young, G. P. Steven, and Y. M. Xie, "Computational efficiency and validation of bi-directional evolutionary structural optimisation," *Computer Methods in Applied Mechanics and Engineering*, vol. 189, no. 2, pp. 559–573, Sep. 2000.

[28] X. Y. Yang, Y. M. Xie, G. P. Steven, and O. M. Querin, "Bidirectional evolutionary method for stiffness optimization," *AIAA Journal*, vol. 37, no. 11, pp. 1483–1488. 1999.